Response to referees' comments

We thank the two anonymous referees for their constructive comments. Since both referees had similar concerns about the lack of lateral drag in the model, we reply to both reviews below. The referees' comments are printed in blue and our response is in black.

Anonymous referee #1:

This is an appealing manuscript. However, I see a very serious flaw in their hypotheses preventing to my opinion acceptance of the proposed manuscript and an in depth re- view. In section 2.2, authors compare lateral drag, longitudinal drag and driving stress to conclude that lateral drag is negligible -not a surprise for this part of Thwaites ice shelf- and is therefore neglected in their model ("we conclude that neglecting the lateral drag in our 2D model is not a major limitation"). To my understanding of the manuscript, this means that there is no parameterization of buttressing in their 2D flow-line modeling attempt. This is indeed a drastic limitation to any investigation of ice shelf perturbations and related impact on grounded ice flow! This is clearly stressed in Schoof (2007) section 4.2:"We now turn to the main limitation of our model, namely that it describes only a two-dimensional ice sheet. This restriction allows us to decouple the evolution of the shelf from the problem of grounded ice flow... Moreover, changes to a two-dimensional ice shelf, for instance through basal melting, DO NOT AFFECT THE GROUNDED ICE SHEET". This was also verified numerically using a full-Stokes model in Gagliardini et al. 2010. Therefore, the design of their entire set of experiments is inconsistent with well-grounded knowledge. So, this would require first demonstrating that previous works have been incorrectly established before embarking in any further discussion on the impact of ice shelf perturbations on grounded ice.

Anonymous referee #2:

*This is an interesting and potentially useful study since both processes are very important and should be included in models predicting future changes in Antarctic glaciers. However, lateral drag is neglected in the 2D model and the paper states that this is not a major limitation (see section 2.2, page 3). But without lateral drag it appears that the effects of buttressing are not parameterised and so any changes in ice shelf due to melting or crevassing would not be propagated upstream and hence not affect the grounding line position. This is at odds with many previously published studies such as Schoof (2007); Gagliardini et al. (2010), who also used a Full Stokes model (e.g. "studying the effect of melting in a plane strain problem with no lateral resistance may lead to unrealistic results"), as also described by RC1. The results in section 4 clearly show this is not the case, at least for the FS model: significant grounding line retreat is seen as basal melt conditions are varied (see figure 8b), so the ice shelf *does* have an effect on the grounded ice. Since it is not clear either to me* *or the other reviewer how this is possible for the model described, could the authors please provide clarification on this point before we proceed, since it is of fundamental importance to assessing the manuscript?*

Both reviewers are absolutely right. With no lateral drag, changes in ice shelf thickness should not affect the position of the grounding line, because the ice shelf is not buttressing grounded ice. In our model, we applied basal melting over the entire ice shelf, and to the first grounded element to simulate a "grounding zone". Changes in the melt rates in this grounding zone is responsible for the sensitivity of the model to melt rates that was described in the first version of our manuscript. To avoid any confusion, we decided to break this manuscript into two papers. The current manuscript will focus only on the propagation of crevasses. Another manuscript focusing on grounding line migration in response to enhanced basal melting within the grounding zone will be submitted later.

To address the referees' comments, we first further validated our implementation of grounding line dynamics in ISSM. We performed the MISMIP hysteresis experiment (Exp 3) to compare our model results with other models (Pattyn et al., 2012). The results is shown in Fig. 5 in the manuscript. The steady state grounding line position obtained with by our model is in good agreement with the FS solution obtained by Elmer/Ice (Pattyn et al., 2012; Durand et al., 2009). The results are also consistent with the analytical solution of Schoof (2007). We attribute the small difference to differences in mesh resolution (Durand et al., 2009; Pattyn et al., 2012). We also tried to reproduce the results of Gagliardini et al. (2010) to test the implementation of the parameterization of the lateral drag with the geometry of MISMIP Exp 1 and the basal melt rate parameterization as Exp 2-c in Gagliardini et al. (2010). The results are shown in Fig. 1 below. Without lateral drag, the grounding line does not retreat when basal melting is applied only on floating ice, as expected. When lateral drag is introduced, the grounding line retreats more than 30 km, which is consistent with the result in Gagliardini et al. (2010) (Fig. 1).

We made the following specific changes to the manuscript:

- we added parameterization of lateral drag following Gagliardini et al. (2010)
- we removed basal melting under grounded elements
- we removed the sections that were related to the basal melting experiments
- we added a figure showing the results of MISMIP Exp 3 (Fig. 5), in order to validate our implementation of grounding line dynamics
- we updated the figures with the implementation of lateral drag (Fig. 6-8)
- we added a simple description of the lateral drag parameterization (Page 4, line 9-13) and the MISMIP experiment (Page 6, line 14-20).

- we also modified the discussion to better describe our results.

References

Durand, G., Gagliardini, O., de Fleurian, B., Zwinger, T., and Le Meur, E.: Marine ice sheet dynamics: Hysteresis and neutral equilibrium, J. Geophys. Res., 114, 1–10, doi: 10.1029/2008JF001170, 2009.

Gagliardini, O., Durand, G., Zwinger, T., Hindmarsh, R. C. a., and Le Meur, E.: Coupling of ice-shelf melting and buttressing is a key process in ice-sheets dynamics, Geophys. Res. Lett., 37, 1–5, doi:10.1029/2010GL043334, 2010.

Pattyn, F., Schoof, C., Perichon, L., Hindmarsh, R. C. a., Bueler, E., de Fleurian, B., Durand, G., Gagliardini, O., Gladstone, R., Goldberg, D., Gudmundsson, G. H., Huybrechts, P., Lee, V., Nick, F. M., Payne, a. J., Pollard, D., Rybak, O., Saito, F., and Vieli, A.: Results of the Marine Ice Sheet Model Intercomparison Project, MISMIP, The Cryosphere, 6, 573–588, doi:10.5194/tc-6-573-2012, URL `http://www.the-cryosphere.net/6/573/2012/`, 2012.

Schoof, C.: Ice sheet grounding line dynamics: Steady states, stability, and hysteresis, J. Geophys. Res., 112, 1–19, doi:10.1029/2006JF000664, 2007.

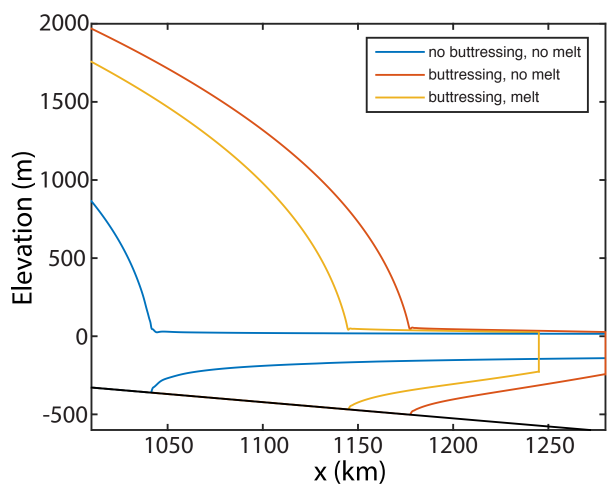

Figure 1: Steady state profiles for the lateral drag validation experiments. Result for the initial MISMIP Exp 1 with no lateral drag and no basal melt is shown in blue. Result with lateral drag and no basal melt is in orange. Result with lateral drag and basal melt rate applied following Exp 2-c (Gagliardini et al., 2010) is in yellow.

~~Full-Stokes modeling of grounding line dynamics, ice melt and iceberg~~ Iceberg calving ~~for~~ of Thwaites Glacier, West Antarctica: Full-Stokes modeling combined with linear elastic fracture mechanics

Hongju Yu[1], Eric Rignot[1,2], Mathieu Morlighem[1], and Helene Seroussi[2]

[1]Department of Earth System Science, University of California, Irvine, Irvine, CA, USA
[2]Jet Propulsion Laboratory, California Institute of Technology, Pasadena, CA, USA

Correspondence to: Hongju Yu (hongjuy@uci.edu)

Abstract. Thwaites Glacier (TG), West Antarctica, has been losing mass and retreating rapidly in the past ~~three~~ few decades. Here, we present a study of its calving dynamics combining a two-dimensional ~~, Full-Stokes~~ flowband Full Stokes (FS) ~~modeling study of the grounding line dynamics and iceberg calving of TG. First, we compare FS with two simplified models,~~ model of its viscous flow with linear elastic fracture mechanics (LEFM) theory to model crevasse propagation and ice fracturing. We compare the results with those obtained with the higher-order (HO) ~~model~~ and the shallow-shelf approximation (SSA) ~~model, to determine the impact of changes in ice shelf basal melt rate on grounding line dynamics. Second, we combine FS with the Linear Elastic Fracture Mechanics (LEFM) theory to simulate crevasse propagation and iceberg calving. In the first experiment, we~~ models coupled with LEFM. We find that FS~~requires basal melt rate consistent with remote sensing observations to reach steady state at TG's current geometry while HO and SSA require unrealistically high basal melt rate. The grounding line of FS is also more sensitive to changes in basal melt rate than HO and SSA. In the second experiment, we find that only FS can produce~~ /LEFM produces surface and bottom crevasses that match ~~radar sounding observations of crevasse width and height~~the distribution of crevasse depth and width observed from NASA's Operation IceBridge radar depth sounders, whereas HO/LEFM and SSA/LEFM do not generate crevasses that match observations. We attribute the difference to the non-hydrostatic ~~conditions~~ condition of ice near the grounding line, which ~~facilitate crevasse formationand are not accounted for in HO and SSA . Additional experiments using FS indicate that iceberg calving is significantly enhanced when surface crevasses exist near the grounding line, when~~ facilitates crevasse formation, and is accounted for by the FS model but not by the HO or SSA model. We also find that calving is enhanced when pre-existing surface crevasses are presenced, when the ice shelf is shortened ~~,~~ or when the ice shelf front is undercut. The role of undercutting depends on the time scale of calving events. It is more prominent for glaciers with rapid calving rates than glaciers with slow calving rates. Glaciers extending into a shorter ice shelf are more vulnerable to calving than glaciers developing a long ice shelf, especially as the ice front retreats close to the grounding line region, which leads to a positive feedback. We conclude that ~~FS~~ the FS/LEFM combination yields substantial improvements in capturing the stress field near the ~~description of ice flow dynamics at the~~ grounding line ~~under high basal melt rate and in~~ for constraining crevasse formation and iceberg calving.

1 Introduction

Thwaites Glacier (TG) is the second largest and broadest ice stream in the Amundsen Sea Embayment (ASE) sector of West Antarctica (Fig. 1). Recent observations have ~~found~~ reported significant thinning and retreat of this glacier (Rignot, 2001; Shepherd et al., 2002; Pritchard et al., 2009; Rignot et al., 2014). ~~Its mass balance~~ The mass balance of Thwaites was -34±16 Gt/yr in 2007 and this value has been decreasing until present to reach -50 Gt/yr in 2013 (Rignot, 2008; Shepherd et al., 2012; Mouginot et al., 2014). ~~In addition, its grounding line has retreated up to~~ Its grounding line retreated 14 km from 1992 to 2011 (Rignot et al., 2014). The bed elevation of the vast majority of ~~the drainage basin of TG~~ its drainage basin is well below sea level and decreases ~~further~~ inland (Tinto and Bell, 2011; Rignot et al., 2014). Such a bed configuration ~~is potentially~~ makes the glacier unstable according to the marine ice sheet instability (MISI) theory (Weertman, 1974; Hughes, 1981; Schoof, 2007). ~~Even with the buttressing of its ice shelf~~ With only a small ice shelf able to buttress it, TG may ~~still undergo a rapid collapse , some of which may already started (Parizek et al., 2013; Joughin et al., 2014)~~already be in a state of collapse (Parizek et al., 2013; Joughin et al., 2014). As the glacier retreats farther inland and loses its floating section, its rate of iceberg calving will rise, which will increase the glacier's contribution to sea level rise (Deconto and Pollard, 2016). It is therefore essential to better understand ~~its dynamics and potential impact on global sea level.~~ and simulate the calving dynamics of TG.

~~The rapid retreat and mass loss of TGhave been attributed to high basal melting and iceberg calving (Depoorter et al., 2013; Rignot et al.,~~ ~~The strengthening and poleward shift of the westerly winds may have brought more warm Circumpolar Deep Water (CDW) toward the ASE than in the past (Spence et al., 2014), which increased basal melting and caused the ice shelf to thin and the grounding line to retreat (Joughin et al., 2012; Rignot et al., 2013).~~ Large calving events have been observed ~~near the grounding line by satellites and densely distributed~~ on the floating section of TG (Fig. 1b) by satellites (MacGregor et al., 2012). Densely distributed surface and especially bottom crevasses have been revealed by ~~ice radar~~ radar depth sounders on the ice ~~shelf of TG~~ (Fig. 2~~, Gogineni (2012)). Both the retreat of grounding line and the shortening of ice shelf reduce ice shelf buttressing and facilitate further retreat (Jenkins et al., 2010; Jacobs et al., 2011; Docquier et al., 2014; MacGregor et al., 2012).~~

~~The grounding line region is key to the stability of marine-terminating glaciers, but it is difficult to simulate numerically because the sharp transition from grounded ice to floating ice involves a complex stress field (Vieli and Payne, 2005; Nowicki and Wingham~~ ~~A Full-Stokes (FS) model is required in this region to capture the flow dynamics accurately (Durand et al., 2009b; Morlighem et al., 2010). Yet, most previous modeling studies of TG used simplified models (Parizek et al., 2013; Docquier et al., 2014; Joughin et al., 2014). Iceberg calving is another process that is difficult to simulate due to the absence of~~). As the buttressing ice shelf calves away and the grounding line retreats, the resistance to flow or buttressing force will decrease, which will favor further retreat and glacier speed up (MacGregor et al., 2012). The calving of icebergs is a difficult process to model because the role of each process is unclear and a universal calving law ~~. Most previous~~ is missing. Most prior studies of crevasse propagation follow the work of Nye (1957), where crevasse ~~propagation is~~ propagates based on the balance between longitudinal stress and ice overburden pressure ~~(Nick et al., 2013; Cook et al., 2014)~~(Bassis and Walker, 2012; Nick et al., 2013; Cook et al., 2014). Although this criterion helps reproduce ice front calving, it does not take into account the stress concentration at the ~~crevasse~~

~~tip~~rupture tips of crevasses and underestimates the depth of crevasses (Bassis and Walker, 2012; Plate et al., 2012). To simulate crevasse propagation at the rupture tip, it is necessary to use the linear elastic fracture mechanics (LEFM) theory ~~(van der Veen, 1998a, b; Krug et al., 2014).~~ (van der Veen, 1998a, b; Larour et al., 2004b; Krug et al., 2014). In order to obtain a description of the stresses that control crevasse propagation in a time dependent fashion, one approach is to model the viscous flow of the ice using an ice flow model and employ the LEFM theory for crevasse propagation.

In this work, we present a ~~Full-Stokes~~ modeling study of the ~~grounding line region~~ calving dynamics of TG using the Ice Sheet System Model (ISSM) ~~framework~~ (Larour et al., 2012) constrained by remote sensing observations~~(Larour et al., 2012)~~. The model is conducted in two dimensions (2D) along a flowline~~of TG. In the first part, we compare the performance of FS with simplified models at reproducing the ice flow of TG near the grounding line. The basal melt rate is adjusted until the glacier achieves steady state conditions with its current geometry . The results are compared with basal melt rate calculated from mass conservation. We then compare the response of TG to enhanced basal melting with FS and simplified models. In the second part of the study, we combine FS~~ , with geometry based on remote sensing observations. We combine various ice flow models with the LEFM theory to investigate crevasse propagation and iceberg calving. We compare the calving behavior of TG using different initial geometries and different levels of complexity of the numerical ice flow models used to calculate the stress field. We conclude on the importance of using FS for modeling the ~~grounding line dynamics and~~ calving processes of TG and the conditions that are conducive to calving.

2 Data and Methods

2.1 Data

~~We~~ To model the glacier in 2D, we select a flowline at the center of the fast ~~flow~~ flowing region of TG as shown in Fig. 1. The flowline is 238 km long~~with~~ , with a 38 km ~~of~~ long floating ice tongue (Fig. 3). BEDMAP-2 is used for ~~surface elevation, bathymetry, and bedrock~~ ice surface, ice bottom and bed elevation (Fretwell et al., 2013). ~~On~~ Over grounded ice, ~~bed elevation from Bedmap2~~ the bed elevation is replaced by the bed elevation computed from ~~mass conservation~~ a mass conservation method (Morlighem et al., 2011, 2013). At the grounding line, the two datasets display ~~some discrepancies~~ discrepancies in the order of hundreds of meters in a few places, but not along the particular flowline that we selected. The ice temperature field is ~~set to the steady-state~~ the steady state temperature computed from the thermal model in ISSM ~~(Larour et al., 2012). This~~ (Larour et al., 2012; Seroussi et al., 2013). The thermal model is constrained by surface temperature from the regional atmospheric climate model RACMO2 (Lenaerts et al., 2012) and geothermal heat flux from Maule et al. (2005) ~~,~~ and includes both conduction and advection processes (Morlighem et al., 2010; Seroussi et al., 2013). The ice surface velocity ~~is~~ derived from interferometric synthetic aperture radar (InSAR) data collected in 2008 is also used to constrain our model (Rignot et al., 2011b).

The NASA Airborne Topographic Mapper (ATM) (Krabill, 2014) surface elevation data and the CReSIS MCoRDS ice thickness data (Gogineni, 2012) provide ice surface and ice shelf bottom elevation, respectively, along flight tracks. We use these observations to compare with our modeling results. Firn correction is applied to each flight track to ensure that the hydrostatic ice bottom calculated from surface elevation matches the observed ice bottom along the ice shelf. Fig. 2 shows the echograms of two flight tracks along the ice shelf of TG, superimposed by the bed picks from CReSIS, surface from ATM and the hydrostatic ice bottom calculated from these datasets.

2.2 Ice Flow Model

~~This work is performed on a~~ The simulations are performed on a 2D flowband model. The ~~velocity gradient across our selected flowline in the grounding line region is small, which implies a small lateral drag. The comparison of lateral drag, longitudinal drag, basal drag and driving stress is shown in Fig. 5. The lateral drag, longitudinal drag and driving stress are computed as in (Van der Veen and Whillans, 1996) from the velocity, geometry and temperature field that we use to initialize the model. The basal drag is computed using the inferred FS basal friction coefficient (Section 2.4). The results are smoothed to 5 km resolution to remove large spatial variations. From 30 km upstream of the grounding line to the ice front, the lateral drag is approximately 18% of the longitudinal drag and 20% of the basal drag over grounded ice . In the vicinity of grounding line, it is about 10% of the longitudinal drag. The longitudinal drag and basal drag also balance well with the driving stress in this region. Further upstream, the lateral drag is in the same magnitude of the longitudinal drag and the basal drag because of the convergence of ice , but the ice is slow compare to the grounding line region and its influence to grounding line dynamics is small. Therefore, we conclude that neglecting the lateral drag in our 2D model is not a major limitation. For completeness, we summarize the~~ basic equations used in our simulations are summarized here for completeness. The ice is considered as an incompressible viscous material driven by gravity. The governing equations of this system are the conservation of momentum and mass:

$$\nabla \cdot \boldsymbol{\sigma} + \rho_i \boldsymbol{g} = \boldsymbol{0} \tag{1}$$

$$\nabla \cdot \boldsymbol{v} = 0 \tag{2}$$

where $\boldsymbol{\sigma}$ is the stress tensor, ρ_i the ice density, $\boldsymbol{g}$ the gravitational acceleration, and $\boldsymbol{v}$ the ice velocity. The deformation of ice under stress is described by the constitutive law:

$$\boldsymbol{\sigma}' = 2\mu\dot{\boldsymbol{\varepsilon}} \tag{3}$$

where $\boldsymbol{\sigma}' = \boldsymbol{\sigma} + p\mathbf{I}$, is the deviatoric stress, p the ice pressure, $\mathbf{I}$ the identity matrix, μ the ice viscosity, and $\dot{\boldsymbol{\varepsilon}}$ the strain rate tensor. The ice viscosity μ is non-linear and follows Glen's law (Glen, 1955):

$$\mu = \frac{B}{2\dot{\varepsilon}_e^{\frac{n-1}{n}}} \tag{4}$$

where B is the ice viscosity parameter, $\dot{\varepsilon}_e$ the effective strain rate, and n the Glen's law exponent. Here, B is a function of ice temperature with value ~~taken~~ interpolated from Cuffey and Paterson (2010) and the Glen's law exponent n is set to 3.

For a 2D flowband model, with ~~x, z~~ (x,z) the horizontal and vertical directions, ~~u, w~~ (u,w) the horizontal and vertical velocities, respectively, the above equations can be rewritten as:

$$\frac{\partial}{\partial x}\left(2\mu\frac{\partial u}{\partial x}\right)+\frac{\partial}{\partial z}\left(\mu\frac{\partial u}{\partial z}+\mu\frac{\partial w}{\partial x}\right)-\frac{\partial p}{\partial x}=0 \tag{5}$$

$$\frac{\partial}{\partial x}\left(\mu\frac{\partial u}{\partial z}+\mu\frac{\partial w}{\partial x}\right)+\frac{\partial}{\partial z}\left(2\mu\frac{\partial w}{\partial z}\right)-\frac{\partial p}{\partial z}-\rho_i g=0 \tag{6}$$

$$\frac{\partial u}{\partial x}+\frac{\partial w}{\partial z}=0 \tag{7}$$

This set of equations is the 2D Full-Stokes model ~~, which does not make any approximation on the stress field of the flowband but~~ and is computationally expensive. To reduce the computational cost, simplified models ~~with approximations are developed~~may be employed.

There are two widely used simplified models. The first one is the higher-order (HO) model (Blatter, 1995; Pattyn, 2003), which assumes that the horizontal gradient of vertical velocity and the bridging effect are negligible (van der Veen and Whillans, 1989). The governing equations are ~~therefore~~ reduced to:

$$\frac{\partial}{\partial x}\left(4\mu\frac{\partial u}{\partial x}\right)+\frac{\partial}{\partial z}\left(\mu\frac{\partial u}{\partial z}\right)-\rho_i g\frac{\partial s}{\partial x}=0 \tag{8}$$

where s is the ice surface elevation. The vertical velocity w is decoupled from the system and is computed from incompressibility.

The second model is the Shallow-Shelf Approximation (SSA) model, which makes the ~~further~~ additional assumption that the vertical shear is negligible (MacAyeal, 1989). This leads to the following 1D model:

$$\frac{\partial}{\partial x}\left(4H\bar{\mu}\frac{\partial u}{\partial x}\right)-\rho_i g H\frac{\partial s}{\partial x}=0 \tag{9}$$

where H is the ice thickness and $\bar{\mu}$ the depth-averaged viscosity.

At each time step, the geometry of the flowband is updated by a mass transport model ~~based on~~ using mass conservation. For FS, the ice surface and ice shelf bottom are treated as two independent free surfaces ~~and~~ updated separately:

$$\frac{\partial z_j}{\partial t}+u_j\frac{\partial z_j}{\partial x}-w_j=\dot{m}_j \tag{10}$$

where the subscript j refers to either the ice surface $(j=s)$ or the ice shelf bottom $(j=b)$ and $\dot{m}_j$ is either the surface mass balance $(j=s)$ or the basal melt rate $(j=b)$. In HO and SSA, only the ice thickness needs to be updated because the ice shelf is assumed to be in hydrostatic equilibrium:

$$\frac{\partial H}{\partial t}+\nabla\cdot(H\bar{\boldsymbol{v}})=\dot{m}_s-\dot{m}_b \tag{11}$$

where $\bar{\boldsymbol{v}}$ is the depth-averaged velocity.

~~In~~ Lateral drag has to be parameterized in a flowband model~~, the~~. Here, it is represented by adding a body force on the ice shelf in the governing equation, as in Gagliardini et al. (2010):

$$f=-\frac{(n+1)^{\frac{1}{n}}B}{2^{\frac{1}{n}}W^{\frac{n+1}{n}}}u^{\frac{1}{n}}; \tag{12}$$

where W is the width of glacier. The convergence of ice from upstream to downstream also needs to be taken into account to conserve mass. Here, we first calculate the ice mass flux along the flowline. Then, we add an artificial surface mass balance term, $\dot{m}_a$, to the original surface mass balance, $\dot{m}_s$, to ensure that the ice mass flux is constant from the inflow boundary to the grounding line.

2.3 Boundary ~~Condition~~Conditions

At the ice surface, the atmospheric pressure exerted on ice is negligible and thus a stress free boundary condition is applied:

$$\boldsymbol{\sigma} \cdot \mathbf{n} = 0 \tag{13}$$

where $\mathbf{n}$ is the unit normal vector pointing outward.

At the bed, boundary conditions are different for grounded ice and floating ice. For grounded ice, the basal drag is assumed to follow a linear friction law:

$$\boldsymbol{\tau_b} = -\alpha^2 \boldsymbol{v}_b \tag{14}$$

where $\boldsymbol{\tau_b}$ is the basal drag, $\boldsymbol{v}_b$ the velocity tangential to the bed, and α the friction coefficient. Here, α is inferred from an inversion so that the modeled surface velocity matches ~~observations~~ observed surface velocity (Section 2.4).

At the ice shelf bottom and ~~at~~ the ice front, seawater pressure is applied at the ice-ocean boundary:

$$\boldsymbol{\sigma} \cdot \mathbf{n} = 0 \qquad z \geq 0 \tag{15}$$

$$\boldsymbol{\sigma} \cdot \mathbf{n} = \rho_w g z \, \mathbf{n} \qquad z < 0 \tag{16}$$

where ρ_w is the seawater density and sea level is at $z = 0$. In our simulations, the ice shelf bottom elevation, $z_b(t)$, is unknown when applying this boundary condition. A replacement with $z_b(t - dt)$, with dt the time step, produces large vertical velocities that destabilize the system (Durand et al., 2009a). ~~A~~ Therefore, a shelf dampening term based on ice velocity and geometry is ~~therefore~~ added to $z_b(t - dt)$ to approximate $z_b(t)$:

$$z_b(t) = z_b(t - dt) + \boldsymbol{v} \cdot \mathbf{n} \sqrt{1 + (\partial z_b(t - dt)/\partial x)^2}\, dt \tag{17}$$

~~At the inflow boundary, a Dirichlet boundary condition is applied for velocity. The horizontal velocity is taken from InSAR-derived ice velocity data (Rignot et al., 2011b) and the vertical velocity is set to 0.~~

2.4 ~~Grounding Line Migration~~

The grounding line position is computed at every time step. ~~The methods used to migrate the grounding line are different for FS and the simplified models.~~ For FS, it is treated as a contact problem (Nowicki and Wingham, 2008; Durand et al., 2009b; Drouet et al., 2013). At ~~each node on~~ the ice-bedrock boundary, the ~~normal stress exerted by the ice is compared to ocean water pressure . If the water pressure~~ grounding line will retreat if the water pressure is higher than the normal stress ~~, the~~

~~corresponding node will be marked as floating and the grounding line will retreat. For the nodes at the~~ exerted by the ice. At the ice-ocean boundary, a non-penetration condition is imposed. ~~If the ice bottom elevation computed from the mass transport model is deeper than the bed elevation, the ice will reground and the grounding line will advance.~~

For HO and SSA, ~~because the governing equations are simplified, the computed stress field cannot accurately represent the actual stress condition near the grounding line and the ice shelf has to be in hydrostatic equilibrium . Therefore, ice is floating if its thickness, H, is smaller than its floating height, H_f:~~

$$\underline{H_f = -\frac{\rho_w}{\rho_i} r_f}$$

~~where r_f is the bedrock elevation. The grounding line position is at the location where $H = H_f$~~ the migration of grounding line is determined by the hydrostatic equilibrium (Seroussi et al., 2014). At the inflow boundary, a Dirichlet boundary condition is applied for the velocity. The horizontal velocity is taken from InSAR-derived ice velocity data (Rignot et al., 2011b) and the vertical velocity is set to 0.

2.4 Inversion for Basal Friction

~~There is~~ We have no direct observation of basal friction. In order to have a realistic representation of the basal conditions, we use an adjoint method ~~, following Morlighem et al. (2010, 2013) ,~~ as in Morlighem et al. (2010, 2013) to find a distribution of the basal friction coefficient, α, that minimizes ~~the~~ a cost function:

$$\mathcal{J}(u,\alpha) = \underline{c_1} \int_{\Gamma_s} c_1 \frac{1}{2}(u-u_{obs})^2 \, d\Gamma + \underline{c_2} \int_{\Gamma_s} c_2 \frac{1}{2} \ln\left(\frac{|u|+\epsilon}{|u_{obs}|+\epsilon}\right)^2 d\Gamma + \underline{c_3} \int_{\Gamma_b} c_3 \frac{1}{2}\left(\frac{\partial \alpha}{\partial x}\right)^2 d\Gamma \tag{18}$$

where u is the modeled surface velocity, u_{obs} the observed surface velocity, ϵ a minimum value (10^{-8} m/yr) to avoid zero velocity, Γ_s and Γ_b the ice surface and bedrock, respectively. The first term of this cost function represents the misfit between modeled and observed velocity. The second term allows a better representation ~~of slow~~ for slow flow regions and the third term is a Tikhonov regularization term ~~to avoid short-scale~~ that avoid unphysical short scale spatial variations of α (Vogel, 2002). ~~The three parameters~~ We calibrate c_1 ~~,~~ and c_2 ~~,~~ so that the first and second terms have the same order of magnitude and we calibrate c_3 ~~are tuned so that we obtain the best fit between modeled and observed surface velocity~~using an L-curve analysis approach.

2.5 Linear Elastic Fracture Mechanics Model

A ~~physically based~~ physically-based LEFM model is used to simulate crevasse propagation. In the LEFM theory, there are three modes to open a crevasse: mode I opening, mode II sliding and mode III tearing. Only mode I is considered here. The key variables in ~~the LEFM model~~ LEFM are the stress intensity factor K and the fracture toughness K_c. If K is larger than K_c, a crevasse will propagate. K is computed through the integration of the normal stress from the bottom of the crevasse to the tip of the crevasse (van der Veen, 1998b). For bottom crevasses, ~~we have~~the equations are:

$$K = \int_{b}^{b+h} \frac{2\sigma_n(z)}{\sqrt{\pi h}} G(z,h,H) dz \tag{19}$$

$$\sigma_n(z) = \sigma_{xx}(z) + \rho_w g z - \rho_i g (s - z) \tag{20}$$

where h is the height between the tip and the bottom of the crevasse, b the elevation of the ice shelf bottom, H the ice thickness, σ_{xx} the longitudinal stress, and G a weighting function (Krug et al., 2014). For surface crevasses, the equations are similar with the water pressure term equals to zero since we assume no melt water production at the surface. K_c is a material property and previous studies showed that K_c ranges from 0.1 to 0.4 MPa m$^{1/2}$ for ice (Fischer et al., 1995; Rist et al., 1996, 2002). Here, K_c is set to 0.2 MPa m$^{1/2}$ ~~,~~ following Krug et al. (2014).

A simple algorithm for the combination of ISSM and ~~the LEFM model~~ LEFM is described in Fig. 4. First, ~~an initial position for a crevasse to form~~ a position is chosen arbitrarily ~~. Then, ISSM is called to compute~~ as the initial crevasse position. ISSM is used to calculate the stress field. With ~~the stress field~~ this stress field at the location of the initial crevasse, the LEFM ~~model is called~~ theory is used to find the maximum ~~height~~ heights of the surface and bottom crevasses that ~~satisfies~~ satisfy $K > K_c$. The geometry is then updated to ~~represent~~ include the propagation of ~~crevasses. After that, the~~ these crevasses. The new ice geometry is allowed to adjust with ISSM for a period of ~~time,~~ 0.01 yr ~~here,~~ during which the crevasse becomes wider, shallower, and smoother due to ~~the~~ viscous deformation of ~~ice. Then the~~ the ice. The LEFM model is ~~called again and we test if new crevasses can~~ then called again to test if the crevasses can still propagate at the center of the existing surface and bottom crevasses. Calving is assumed to occur when either the surface or the bottom crevasse reaches sea level (Benn et al., 2007).

3 Simulations

3.1 ~~Model setup~~FS model evaluation

ISSM is a coupled, thermo-mechanical, finite element, ice flow model (Larour et al., 2012). The three models, FS, HO and SSA are ~~all~~ implemented in ISSM, which makes it ~~a practical tool~~ practical to compare their performance (Morlighem et al., 2010; Seroussi et al., 2011).

~~We choose a horizontal mesh resolution of 100 m to obtain a precise description of the grounding line position (Durand et al., 2009b). In the vertical direction,~~ To evaluate the FS model, we conduct the Experiment 3 of MISMIP, which is a model comparison experiment that evaluates the migration of grounding line in response to changes in ice rheology on an over-deepened bed (Pattyn et al., 2012). The result, shown in Fig. 5, indicates that the ~~domain is uniformly divided into 20 layers. In total, the mesh comprises 95,200 triangle elements. An inversion for the basal friction coefficient, α, on grounded ice is first conducted for the selected flowline before any transient simulation is run.~~

3.2 ~~Basal Melting~~

~~With no direct measurement of basal melt rate, the melt rate computed from mass conservation is used as an approximation of the actual basal melt rate, following Rignot et al. (2013). We take two flowlines that are 5 km apart on the ice shelf of TG, with the selected flowline in the center, and calculate the ice mass flux of this band from the grounding line to the ice front. Because the surface thinning rate and surface mass balance in this region is an order of magnitude smaller than the basal melt rate (Pritchard et al., 2009), the decrease of ice flux is assumed to be caused entirely by basal melting. The melt rate computed here is used as the control melt rate for the following experiments.~~

~~Once the control melt rate is computed, we find basal melt rate for each model that provide steady state solutions with the current geometry in a 100-yr simulation, with a time step of 0.1 yr. The basal melt rate is adjusted for each model to ensure that at the end of the simulation, the rate of thickness change is less than 0.05 m~~grounding line is unstable on a retrograde bed and displays a hysteresis behavior in response to perturbations in ice rheology. This is consistent with the MISI theory, the analytical solution and other numerical models (Weertman, 1974; Schoof, 2007; Pattyn et al., 2012). The steady state grounding line positions obtained by ISSM agree with the FS solution obtained by Elmer/~~yr, the grounding line does not migrate and the total change of ice shelf thickness is less than 25 m (Fig. ??b). We then compare the melt rate of each model with the control melt rate.~~

~~Two sets of sensitivity experiments are then conducted where we vary the basal melt rate (Table 1). In the first set, denoted Exp. Ma1–Ma4, we add an additional melt rate, $\dot{m}_{b\_a}$, to the control melt rate as a function of the depth of the ice shelf draft. We impose a maximum melt rate, $\dot{m}_{b0}$, at 50 m/yr, 100 m/yr, 200 m/yr and 300 m/yr, respectively, for Exp. Ma1–Ma4. $\dot{m}_{b\_a}$ is set to equal to $\dot{m}_{b0}$ below -600 m, then linearly decreases to 0 at -200 m and remains 0 above -200 m (Fig. ??a). If the grounding line retreats, the basal melt rate applied on the ungrounded part is the control melt rate at current grounding line (68 m/yr) plus the additional melt rate $\dot{m}_{b\_a}$.~~

Ice (Durand et al., 2009a), within 15 km. The results are also in good agreement with the analytical solution of Schoof (2007), especially in the retreating phase (step 7-13), within 20 km. In the ~~second set, Exp. Mb1–Mb4, we use the basal melt rate that provides steady state for each model (Fig. ??)as the starting point. Then we add the same additional melt rate, $\dot{m}_{b\_a}$, as in Exp. Ma1–Ma4 (Fig. ??). To avoid a large region of over 500 m/yr melt rate for SSA and HO, the melt rate applied for ungrounded region is altered. If the grounding line retreats, the melt rate from the new~~ advancing phase, the difference is larger, ∼50 km. However, this level of discrepancy in grounding line position ~~to 38 km downstream is the initial melt rate along the 38km ice shelf plus $\dot{m}_{b\_a}$ (Fig. ??). Further downstream, only $\dot{m}_{b\_a}$ is applied. The two sets of sensitivity experiments are both run for 40 years for each of the three models.~~ is considered to be satisfactory and has been attributed to numerical issues associated with mesh resolution (Durand et al., 2009a; Pattyn et al., 2012). Therefore, we conclude that ISSM is able to reproduce the results of MISMIP Exp 3.

3.2 ~~Crevasse Propagation~~Model Setup

~~The propagation of crevasses takes place over small spatial and temporal scales. In order to increase the reliability of the model, the mesh is refined accordingly. The~~ In our simulations, the horizontal resolution is ~~increased from~~ 100 m, refined to 5 m within 3 km of the initial crevasse position~~and the number of vertical layers is increased from 20 to 40. The domain is~~

~~therefore discretized into~~ . Vertically, the domain is uniformly discretized into 40 layers. In total, the domain has 281,~~660~~ 680 elements. The time step ~~is shortened from 0.1 yr to~~ we choose is 0.0005 yr (∼4.4 hr) and the LEFM model is called every 0.01 yr. ~~The simulations are run for 0.3 yr or until calving occurs, whichever happens first~~In all the following experiments, the basal melt rate is chosen so that the grounding line does not migrate and the ice shelf bottom has a stable elevation (within few meters).

Five sets of experiments, ~~Exp. Ca–Ce~~labeled Exp. A–E, are conducted to simulate the propagation of crevasses (Table 1). In the first set, eleven experiments, Exp. ~~Ca1–Ca11, are conducted~~ A1–A11, are run with micro initial crevasses, ~~which have both width and height initialized at 0. In all~~ zero crevasse depth and width, at both the surface and the bottom. In these experiments, the ~~experiment~~ number 1–11 indicates the initial crevasse position, respectively, ~~at~~ 0.5~~km~~, 1~~km~~, 1.5~~km~~, 2~~km~~, 2.5~~km~~, 3~~km~~, 3.5~~km~~, 18~~km~~, 28~~km~~, 35 ~~km~~ and 36 km downstream of the grounding line. These positions are chosen to represent~~the~~ , respectively, crevasse propagation near the grounding line, in the middle of the ice shelf, and near the ice front.

In the ~~following~~ next four sets of experiments, the initial geometry is altered to ~~investigate the calving behavior in the grounding line region. In the second set~~ evaluate its impact on crevasse propagation. The second (Exp. ~~Cb1–Cb7) , a 3 m deep, 100 m wide initial surface crevasse is added to the initial geometry while the initial bottom crevasses are still micro crevasses. The~~ B1–B7) and the third (Exp. ~~Cc1–Cc7) and fourth (Exp. Cd1–Cd3)~~ C1–C3) sets are designed to test the stability of TG ~~to~~ with a shortened ice shelf. ~~In these two sets,~~ The length of the ice shelf ~~length is shortened~~ is reduced from 38 ~~km~~ to 4 km (Exp. B) and 2 km (Exp. C), respectively. In the ~~last~~ fourth set (Exp. ~~Ce1–Ce7), we add a 400 m wide and 400 m high undercutting at the ice front on the~~ D1–D7), a 3 m deep, 100 m wide initial surface crevasse is added to the initial geometry while the initial bottom crevasse is still kept as a micro crevasse. In the last set (Exp. E1–E7), we undercut the ice shelf front of a 4 ~~km ice shelf case to investigate the impact of undercutting on calving.~~ km–long ice shelf by 400 m over the last 400 m. The initial crevasse positions for these sets of experiments are the same as Exp. A.

4 Results

4.1 Inversion

~~Results from the inversion~~ The inversion results of FS, HO and SSA are shown in Fig. 6. For all three models, the inferred basal friction coefficient, α, has similar values and spatial patterns. The modeled ~~surface~~ ice surface velocities are in reasonable agreement. The modeled surface velocity after inversion closely matches the observed surface velocity ~~on~~ over grounded ice. ~~There is still~~ However, there remains a 200 m/yr, or 6%, difference in the grounding line region and on the ice shelf. We attribute this discrepancy to ~~the~~ errors in ice rheology ~~field and~~ and uncertainties associated with the parameterization of the ~~lack of~~ lateral drag. ~~Yet, all modeled ice surface velocities are in good agreement, which provides comparable initial conditions.~~

4.2 ~~Basal Melting~~

4.2 Observed crevasses

~~The melt rate computed from mass conservation is shown as “control” in~~ In the data acquired by NASA ATM and CReSIS MCoRDS from 2009 to 2014 (Gogineni, 2012; Krabill, 2014), we find that surface and bottom crevasses are densely distributed on the ice shelf of TG (Fig. 1b and Fig. ~~??a. It is highest within 10 km of the grounding line. The maximum occurs at 2.4 km downstream of the grounding line and reaches 73 m /yr. Further downstream of the grounding line, the melt rate oscillates around~~ 2). With these data, we estimate the height and width of each surface and bottom crevasse (crevasses narrower than 200 m are neglected). We find that the mean height is 18.7 m for surface crevasses and 103.1 m for bottom crevasses. The height of surface crevasse ranges from 2–82 m, but 90 % of them are within 2–40 m. The height of bottom crevasses ranges from 20–270 m. The mean width for surface and bottom crevasses are 821 m and 724 m, respectively, and 80 % of the crevasses have a width ranging from 300 m to 1000 m. The measurement error is 10 m ~~/yr due to the spatial variations in the elevation of the ice shelf bottom .~~

~~The basal melt rate required for FS, HO and SSA to maintain steady state at the current geometry are plotted in Fig. ??a. For all three models, the melt rates are similar and match the control rate except the first 5 km of the ice shelf. Within 5 km of the grounding line, especially the first 3 km, FS is different from HO and SSA. The FS result is similar to the control rate with a peak melt rate of 86 m /yr at 2.5 km downstream of the grounding line, while the results of HO and SSA are unrealistically high: they both require over 500 m /yr melt rates to prevent the grounding line from advancing (Fig. ??a). For FS, we find a 5 km zone~~ for the ATM-derived ice surface elevation (Krabill, 2014) and 14 m for the MCoRDS-derived ice bottom elevation (Gogineni, 2012).

4.3 Non-hydrostatic behaviors

In the grounding line region of TG, i.e. within 5–10 km downstream of the grounding line~~where~~ , the ice is tens of meters below hydrostatic equilibrium (Fretwell et al., 2013). In our selected flowline, the maximum deviation is 85 m. ~~The deviation is of the order of tens of meters with a maximum of 68 mat 400 m downstream of the grounding line.~~

~~The results of the first set of the sensitivity experiments (Exp. Ma1–Ma4) are~~ In the two flight tracks shown in Fig. ~~??. In the control run, the grounding line of FS is stable at its current position and the ice shelf thickens slightly. For HO and SSA, the grounding line positions advance by 3.6 km and 4.9 km, respectively, and the ice shelf thickens by a few hundred meters. With enhanced basal melting compared to the control melt rate, the grounding line position of FS retreats by 42 km, 85 km, 120 km and 124 km, respectively, for Exp. Ma1–Ma4. On the contrary, for HO and SSA, the grounding lines only retreat slightly in Exp. Ma4~~2, we find the maximum deviation to be 130 m for track PQ and 122 m for track RS. In addition, in the positions where surface and bottom crevasses exist, this deviation is larger, measured in hundreds of meters (Fig.

~~In the second set of experiments (Exp. Mb1–Mb4, Fig. ??), the grounding line retreats in every experiment for all models, as expected. However, the sensitivity of grounding line positions to changes in melt rate is different. In FS, the grounding line retreats by 73 km, 115 km, 123 km and 127 km for Exp. Mb1–Mb4, respectively. For HO and SSA, the grounding line retreat~~

~~is the same for all four experiments, 37 km for HO and 21 km for SSA. In both sets of sensitivity experiments, along with the grounding line retreat, strong surface thinning and mass loss are produced in the entire domain for FS. However, despite the similarity in ice shelf thinning, the grounded ice thinned significantly less for HO and SSA.~~

~~To summarize, only FS can reach~~ 2). In the FS solution of ISSM, this non-hydrostatic condition can be simulated. For instance, we get a maximum of 68 m deviation in a steady state ~~with realistic values of the magnitude of basal melting and capture the current grounding line position. The simplified models, HO and SSA, require high basal melt rates near the grounding line and are also less sensitive to changes in basal melt rate.~~ solution for our selected flowline.

4.4 Crevasse ~~Propagation~~propagation

In all crevasse propagation experiments with HO and SSA, we find that the height of ~~bottom crevasses~~ a bottom crevasse never exceeds 50 m, which is small compared to observations~~and does not~~. At the end of the simulations, the crevasses never grow enough to produce a calving event. In other words, ~~if~~ under the assumption of hydrostatic equilibrium~~is used for the ice shelf~~, which is required, HO and SSA are unable to grow crevasses that ~~can generate calving using~~ generate calving events when combined with the LEFM theory. In the remainder of the ~~paper~~study, we only discuss the FS case.

In the first set of experiments (Exp. ~~Ca1–Ca11), based on~~ A1–A11), with the initial geometry and ~~the introduction of micro crevasses at both the surface~~ micro crevasses on the top and the bottom of the ice shelf, the crevasses of all eleven cases stop growing at the end of the ~~experiments and none of them produce calving~~ simulations and none produce a calving event (Fig. 7). The final height of bottom crevasses is 200–300 m near the grounding line (Exp. ~~Ca1–Ca7~~A1–A7) and 50–100 m downstream (Exp. ~~Ca8–Ca11~~A8–A11). The surface crevasses are one order of magnitude smaller, 10–15 m near the grounding line and 2–5 m downstream. The width of all crevasses is ~~400–500~~ between 400 and 500 m.

The results of the experiments with varying initial ~~geometry~~ geometries are shown in Fig. 8. ~~In Exp. Cb1–Cb7, where we add a 3 m surface crevasse at the top of the ice shelf~~ With an ice shelf shortened to 4 km, calving occurs ~~for crevasses located within 1.5~~ within 1 km of the ~~grounding line~~ ice front (Exp. ~~Cb1–Cb3~~B6 and B7, Fig. 8a) ~~. Further downstream of the grounding line~~ and the other experiments (Exp. ~~Cb4–Cb7) , the crevasse propagation is nearly identical to the case with micro initial surface crevasse~~ B1–B5) have results similar to the initial 38 km long ice shelf (Exp. ~~Ca4–Ca7~~A1–A5), i.e. the final bottom crevasse height does not exceed 200–300 m.

With an ice shelf shortened to ~~a length of 4~~ 2 km, calving occurs ~~within 1 km of the ice front~~ in all three experiments (Exp. ~~Cc6 and Cc7~~C1–C3, Fig. 8b)~~and the other experiments (Exp. Cc1–Cc5) have results similar to the initial 38 km long ice shelf (Exp. Ca1–Ca5). With an ice shelf shortened to only 2 km, calving occurs in all three experiments~~.

In Exp. D1–D7, where we add a 3 m deep, 100 m wide, initial surface crevasse, calving occurs for crevasses located within 1.5 km of the grounding line (Exp. ~~Cd1–Cd3~~D1–D3, Fig. 8c). Further downstream (Exp. D4–D7), the crevasse propagation is identical to the case with micro surface crevasses (Exp. A4–A7).

In the last set, where the ice shelf is shortened and undercut~~. We~~, we find that calving occurs within 1.5 km of the ice front (Exp. ~~Ce5–Ce7~~E5–E7, Fig. 8d). In regions where calving does not occur, undercutting vanishes slowly within 0.1 yr due to the viscous deformation and ~~the~~ downstream advection of ice.

~~In all of the above experiments, Exp. Cc6~~ Among all experiments, only Exp. B6 produces calving caused by a surface crevasse propagating to sea level and it takes ~~approximately~~ 0.24 yr for the calving to occur. For all other calving cases, calving occurs because a bottom crevasse propagates to sea level and the process is ~~significantly~~ five times more rapid, ~~within 0.05 yr.~~

5 ~~Discussion~~

4.1 ~~Basal Melting~~

~~Our results show that only FS experience significant grounding line migration and provides a realistic response to enhanced basal melting. With HO and SSA, the basal melt rates have to be unrealistically high near the grounding line,~~ i.e. ~~over 500 m/yr, in order for the models to achieve steady state conditions with the current geometry.~~

~~In the grounding line region, the abrupt change in boundary condition creates a singularity. Most importantly, ice is pushed below hydrostatic equilibrium downstream of the grounding line as a result of a bending moment of the ice. This bending moment does not exist in the simplified models. As a result of the non-hydrostatic conditions, the ice pressure and the vertical velocity are high, which produces high vertical shear stress that tends to lift the ice from the bed. FS is capable of taking into account this high vertical shear stress and makes it possible to migrate the grounding line based on realistic stress conditions. In HO and SSA, bridging effects are neglected and ice is assumed to be in hydrostatic equilibrium, which tend to make the grounding line advance.~~

~~Our sensitivity experiments show that the grounding lines in HO and SSA are much less sensitive to an increase in basal melt rate. In contrast, the FS grounding line is more sensitive to enhanced basal melting and retreats almost in every scenario. On flat or retrograde bed, the migration of the grounding line is similar in all three models. Yet, on a prograde bed, the grounding lines of HO and SSA tend to sit on bedrock bumps unless unrealistic basal melt rate is applied at the grounding line (Fig. **??**– **??**). To retreat over the bump where the current grounding line is at, over 500 m/yr melt rate is required. Even 800 m/yr melt rate is unable to make HO and SSA retreat over the bump 37 km and 21 km upstream of the current grounding line, respectively. However, satellites observations have shown that the grounding line of TG and its neighbor Pine Island Glacier has already retreated over a few bedrock bumps in the past decade under current ocean forcing (Rignot et al., 2014). This suggests that previous studies of TG may have underestimated its response to changes in ocean thermal forcing (Parizek et al., 2013; Joughin et al., 2014)~~

~~In the future, a steady increase in the strength of the westerlies may cause the ocean temperature to rise by more than 2°C. It may also push more ocean heat toward TG without any changes in ocean temperature (Spence et al., 2014). As a result, the basal melting of TG will be enhanced. As the glacier is retreating into an area where the bed elevation is lower, the melt rate will be further increased because of the pressure-dependence of the melting point of the ocean water/ice melange. In Rignot and Jacobs (2002), it is suggested that a 1°C increase in ocean thermal forcing would raise the basal melt rate by 10 m/yr. In Holland et al. (2008), the basal melt rate is suggested to increase quadratically to ocean warming. However, in either case, the basal melt rate of TG would be unlikely to increase by more than 100 m/yr. In our experiments as well as in previous studies, basal melt rate of at least 200 m/yr have been required to push the grounding line out of equilibrium using HO and SSA~~

~~(Parizek et al., 2013; Joughin et al., 2014). If we increase the basal melt rate by a more realistic 50 m/yr, our results suggest that only FS can produce a retreat of the grounding line (Exp. Ma1). Even if we use a high initial basal melt rate for HO and SSA, the response of grounding line to enhanced basal melting is still less sensitive and largely dependent on the bed topography (Exp. Mb1–M4b). We conclude that it may be essential to use FS in the grounding line region for 2D simulationsto correctly represent the impact of ocean thermal forcing on grounding line stability~~within 0.05 yr. For the cases that calving does not take place, the crevasses stop growing before the end of the simulations.

4.1 ~~Crevasse Propagation~~

5 Discussion

The ~~sizes~~ size of surface and bottom crevasses produced ~~from~~ by our crevasse propagation experiments with FS (Fig. 7) are ~~compatible with the size~~ comparable with the sizes of surface and bottom crevasses observed ~~from~~ by ice radar sounders (Fig. 2~~, Gogineni (2012)~~). This suggests that the combination of FS with the LEFM theory is a realistic ~~tool to study~~ way to model crevasse propagation and iceberg calving. ~~However, with~~ With HO and SSA, however, because of the assumption of hydrostatic equilibrium, the water pressure term and the overburden ice pressure term in Eq. (19) cancel ~~out~~ each other at the bottom of the ice shelf and thus the bottom crevasses are unable to grow to a size that matches observations. With the non-hydrostatic condition included, the two pressure terms in Eq. (19) do not cancel each other with FS in the region near the grounding line or the region with crevasses, which helps propagate the crevasses. In the radar echograms, large bottom crevasses (over 100 m) are also observed along the ice shelf, tens of kilometers downstream of the grounding line. ~~We think~~ According to our results from Exp. A, the crevasses formed in the grounding line stop growing once they reach a stable size. Therefore, we posit that these crevasses ~~may be~~ are the result of advection of crevasses ~~from upstream, not from a recent cracking.~~ formed upstream. In summary, the non-hydrostatic condition plays a major role in crevasse formation. Not accounting for this condition makes it difficult to explain the observed crevasse pattern.

In our simulations, we find that crevasses propagate significantly faster near the ~~grounding line when they initiate from a 3-m deep surface crevasse. The existence of such a small crevasse has limited impact on the overall stress field of the ice shelf . The reason that it has an influence on crevasse propagation is that it changes the pressure field. At the ice bottom of the grounding line region, ice is pushed below hydrostatic equilibrium, the longitudinal stress field is small or even compressive. In the first few steps of the simulation, the bottom crevasse does not propagate. During that time, the surface crevasse grows because the surface longitudinal stress is large. The difference between water pressure and the overburden ice pressure keeps increasing at the bottom until the stress intensity factor of the bottom crevasse is larger than its fracture toughness. With an initial surface crevasse, the difference between water and ice pressure is enhanced and the bottom crevasse is then able to propagate through the entire ice thickness and produce calving. In the flowline selected here, we find that 3 m is the minimum initial surface crevasse depth that is required to produce calving. If the non-hydrostatic behavior of the ice is more pronounced, the required minimum height of the surface crevasse will become smaller.~~

ice front when the ice shelf is shortened. In principle, the length of a nearly non-confined ice shelf, such as the floating ice tongue of TG, should not have a major impact on the buttressing that the ice shelf exerts on grounded ice. Here, ~~however,~~ we find that the propagation of crevasse near the ice front~~is limited on~~ , while limited for the initial 38 ~~km ice shelfwhile it is significantly more likely to experience calving~~ km-long ice shelf, becomes significantly enhanced with a shortened ice shelf. When the ice shelf is shortened, the longitudinal stress near the ice front ~~will increase~~ increases at the surface and ~~decrease~~ decreases at the bottom. The increase in the surface stress makes it easier for the surface crevasse to propagate, while the decrease in bottom stress prevents the propagation of the bottom crevasse. As time goes, the ~~bottom stress increases while~~ stress at the bottom increases and the surface crevasse grows. ~~Then the~~ The bottom crevasse is then able to propagate quickly through the entire ice ~~thickness~~ column to cause calving ~~as a result of the~~ because of the large difference between the water pressure and the overburden ice pressure. If calving takes place and creates a shorter ice shelf, our model predicts that the new ice shelf will be more prone to calving, i.e. a positive feedback.

When an initial crevasse of 3 m depth and 100 m width is added to the surface, we find that the surface crevasse grows quickly to 35 m before the bottom crevasse starts to propagate. The large difference between the water pressure and the ~~ice overburden pressure.~~ overburden ice pressure at the bottom however, makes the bottom crevasse propagate rapidly through the entire ice thickness and produces calving. This is consistent with Bassis and Walker (2012), who suggested that ice shelves are difficult to form in the presence of pre-existing crevasses. However, long ice shelves calving at the grounding line region is not something commonly observed on TG. Three reasons might explain this result. One reason is that we assume that a surface crevasse aligns perfectly with a micro-crack at the bottom, which is not certain. A second one is that bottom crevasses could also form from thermal cracking (Humbert and Steinhage, 2011; Vaughan et al., 2012), in particular not aligned with a surface crack. Thermal cracking would facilitate the propagation of a bottom crevasse. If the corresponding surface crevasse remains shallow, the seawater-filled bottom crevasse formed by thermal cracking will not propagate far because the difference between the water pressure and the overburden ice pressure will be smaller than in the presence of a deep surface crevasse. The third reason is that most surface crevasses are formed in train, whereas here we only model one. A train of crevasses creates a shielding effect, which effectively reduces the stress concentration at rupture tips and anneals the propagation of crevasses (van der Veen, 1998b; Krug et al., 2014).

Undercutting on the ice front is a common feature~~for glaciers (Rignot et al., 2010), whose influence on calving is still unclear. O'Leary and Christoffersen (2013) showed~~ , especially for tidewater glaciers with a short to non-existent floating section (Rignot et al., 2010). In a prior study, O'Leary and Christoffersen (2013) suggested that undercutting leads to significant changes in the stress field ~~near the ice front and~~ that enhances calving. Cook et al. (2014) argued, however, that the change in ~~the~~ stress field is only significant in diagnostic simulations and ~~the undercutting influence~~ is much smaller in prognostic simulations. Krug et al. (2015) also showed that undercutting has no effect on the glacier mass balance on annual time scales. Here, we find that undercutting does affect the stress field significantly near the ice front ~~. It~~ but its impact on calving depends on the time scale of calving events. Undercutting increases the surface stress and decreases the bottom stress just ~~like~~ as in the case of a shorter ice shelf and thus induces ~~calving in a similar way. However, the influence is only for a short duration because of the~~ a similar type of calving. The influence of the stress field is however time dependent due to the viscous adjustment of ~~the ice. If~~ ice. In our simulations, we find that if the undercutting is not large enough to produce calving ~~in a short period of time,~~ within about 0.1 yr, then it will have no impact on calving. If ~~it is large and produces calving fast, then we find that undercutting enhances the propagation of crevasses~~calving occurs on shorter time scales, then undercutting significantly enhances the process. This conclusion ~~reconciles the results of the previous studies and~~ effectively reconciles the previous studies because it shows that the impact of undercutting depends on ~~how long the ice shelf front remains undercut before the next calving .~~

5.1 ~~3D modeling~~

~~It would be of interest to generalize the present simulations to a 3D model. We do not think that the results of this study would be significantly changed, but a 3D model would provide a more realistic context for~~ the ~~model and is eventually needed to simulate the evolution of TG in the coming decades to centuries. A~~ time scale of calving events. We conclude that the impact of undercutting will be more significant for fast-moving glaciers with high calving rates than for slow moving glaciers with a low calving rate. A high calving rate will give less time for the glacier to adjust viscously to the undercutting than for a slow calving glacier. As a conjecture, since glaciers with a high calving rate have more impact on the total mass balance, we conclude that undercutting is an important factor in the study of calving dynamics.

In this study, the simulations are all conducted in a 2D flowband model with one crevasse propagation event. It would be of interest to generalize the present simulation to a 3D ~~model would include the impact of the eastern ice shelf, which is buttressed by a series of ice rumples (MacGregor et al., 2013). It would also include a more complete geometry of the bed with series of bumps and hollows. The grounding lines of HO and SSA may be more sensitive to changes in basal melt rate since they can retreat around subglacial bumps. In addition, the simulation of ice shelf rifts, not considered here but studied elsewhere (e. g. Larour et al. (2004a)), would provide an additional~~ geometry with multiple crevasses and a moving ice front. In 3D, a better representation of the lateral shear and a complete surface/bed geometry will provide a more realistic context for the ~~formation of tabular icebergs from the ice shelves in this region.~~

~~Since a FS 3D modeling of TG may not be possible at a high spatial resolution given our current computational constraints, we recommend a hybrid approach such as the one proposed by Seroussi et al. (2012), which uses FS around the grounding line region and employs simplified models in the surrounding regions~~models. The simulation of a series of calving events with a train of crevasses over a long time period would provide more realistic information about how a glacier will respond to a calving event in terms of the migration of its grounding line and the evolution of its ice speed.

6 Conclusions

~~In this study, we~~ We use a two-dimensional flowband Full-Stokes model ~~to study the grounding line dynamics and~~ coupled with LEFM theory to model the calving behavior of TG. We ~~show that only FS is able to reproduce steady state conditions with basal melt rate similar to those deduced from remote sensing observations and only FS produces significant grounding line migration with enhanced basal melting. With HO and SSA, the grounding line tends to advance from the initial position~~

~~and is insensitive to realistic changes in basal melt rate. The explanation is that ice is pushed below hydrostatic equilibrium in that region and only FS is able to account for the~~ find that FS combined with LEFM produces crevasses consistent in width and depth with observations and is capable of producing calving events. The reason for the propagation of crevasse is the existence of non-hydrostatic ~~conditions. In terms of calving dynamics, we show that FS combined with LEFM theory produces crevasses that match observations. We find that the non-hydrostatic~~ conditions of ice near the grounding line ~~significantly facilitate and explain the formation of deep crevasses. Shorter ice shelves, ice shelves with a significant amount of undercutting and ice shelves with surface crevasses appear more vulnerable to calving than long ice shelves, with vertical ice front and no surface crevasse. This work suggests~~ which is not accounted for in simplified models that assume hydrostatic conditions everywhere on the ice shelf. We also find that calving is enhanced in the presence of pre-existing surface crevasses, on shorter ice shelves and if the ice front is undercut. We conclude that it is ~~essential to use FS near the grounding line, to capture the grounding line dynamics correctly and to simulate the propagation of crevasses leading~~ important to consider the full stress field in the grounding line region to properly represent the stress field and replicate the conditions conducive to calving events~~more realistically.~~. Further studies ought to examine how these results may vary in a 3D domain with complete modeling of the role of the lateral margins.

Acknowledgements. This work was carried out at the University of California Irvine and at California Institute of Technology's Jet Propulsion Laboratory under a contract with the Cryosphere Science Program of the National Aeronautics and Space Administration, grant NNX14AN03G.

References

Bassis, J. N. and Walker, C. C.: Upper and lower limits on the stability of calving glaciers from the yield strength envelope of ice, Proceedings of the Royal Society A: Mathematical, Physical and Engineering Sciences, 468, 913–931, doi:10.1098/rspa.2011.0422, 2012.

Benn, D. I., Warren, C. R., and Mottram, R. H.: Calving processes and the dynamics of calving glaciers, Earth Sci. Rev., 82, 143–179, doi:10.1016/j.earscirev.2007.02.002, 2007.

Blatter, H.: Velocity And Stress-Fields In Grounded Glaciers: A Simple Algorithm For Including Deviatoric Stress Gradients, J. Glaciol., 41, 333–344, 1995.

Cook, S., Rutt, I. C., Murray, T., Luckman, a., Zwinger, T., Selmes, N., Goldsack, a., and James, T. D.: Modelling environmental influences on calving at Helheim Glacier in eastern Greenland, Cryosphere, 8, 827–841, doi:10.5194/tc-8-827-2014, 2014.

Cuffey, K. M. and Paterson, W. S. B.: The Physics of Glaciers, 4th Edition, Elsevier, Oxford, 2010.

Deconto, R. M. and Pollard, D.: Contribution of Antarctica to past and future sea-level rise, Nature, 531, 591–597, doi:10.1038/nature17145, http://dx.doi.org/10.1038/nature17145, 2016.

Depoorter, M. a., Bamber, J. L., Griggs, J. a., Lenaerts, J. T. M., Ligtenberg, S. R. M., van den Broeke, M. R., and Moholdt, G.: Calving fluxes and basal melt rates of Antarctic ice shelves., Nature, 502, 89–92, doi:10.1038/nature12567, 2013.

Docquier, D., Pollard, D., and Pattyn, F.: Thwaites Glacier grounding-line retreat: influence of width and buttressing parameterizations, J. Glaciol., 20, 305–313, doi:10.3189/2014JoG13J117, 2014.

Drouet, a. S., Docquier, D., Durand, G., Hindmarsh, R., Pattyn, F., Gagliardini, O., and Zwinger, T.: Grounding line transient response in marine ice sheet models, The Cryosphere, 7, 395–406, doi:10.5194/tc-7-395-2013, 2013.

Durand, G., Gagliardini, O., de Fleurian, B., Zwinger, T., and Le Meur, E.: Marine ice sheet dynamics: Hysteresis and neutral equilibrium, J. Geophys. Res., 114, 1–10, doi:10.1029/2008JF001170, 2009a.

Durand, G., Gagliardini, O., Zwinger, T., Le Meur, E., and Hindmarsh, R. C. A.: Full Stokes modeling of marine ice sheets: influence of the grid size, Ann. Glaciol., 50, 109–114, 2009b.

Favier, L., Gagliardini, O., Durand, G., and Zwinger, T.: A three-dimensional full Stokes model of the grounding line dynamics: effect of a pinning point beneath the ice shelf, The Cryosphere, 6, 101–112, doi:10.5194/tc-6-101-2012, 2012.

Fischer, M. P., Alley, R. B., and Engelder, T.: Fracture toughness of ice and firn determined from the modified ring test, Journal of Glaciology, 41, 383–394, 1995.

Fretwell, P., Pritchard, H. D., Vaughan, D. G., Bamber, J. L., Barrand, N. E., Bell, R., Bianchi, C., Bingham, R. G., Blankenship, D. D., Casassa, G., Catania, G., Callens, D., Conway, H., Cook, a. J., Corr, H. F. J., Damaske, D., Damm, V., Ferraccioli, F., Forsberg, R., Fujita, S., Gim, Y., Gogineni, P., Griggs, J. a., Hindmarsh, R. C. a., Holmlund, P., Holt, J. W., Jacobel, R. W., Jenkins, A., Jokat, W., Jordan, T., King, E. C., Kohler, J., Krabill, W., Riger-Kusk, M., Langley, K. a., Leitchenkov, G., Leuschen, C., Luyendyk, B. P., Matsuoka, K., Mouginot, J., Nitsche, F. O., Nogi, Y., Nost, O. a., Popov, S. V., Rignot, E., Rippin, D. M., Rivera, A., Roberts, J., Ross, N., Siegert, M. J., Smith, a. M., Steinhage, D., Studinger, M., Sun, B., Tinto, B. K., Welch, B. C., Wilson, D., Young, D. a., Xiangbin, C., and Zirizzotti, A.: Bedmap2: improved ice bed, surface and thickness datasets for Antarctica, The Cryosphere, 7, 375–393, 2013.

Gagliardini, O., Durand, G., Zwinger, T., Hindmarsh, R. C. a., and Le Meur, E.: Coupling of ice-shelf melting and buttressing is a key process in ice-sheets dynamics, Geophys. Res. Lett., 37, 1–5, doi:10.1029/2010GL043334, 2010.

Glen, J. W.: The creep of polycrystalline ice, Proc. R. Soc. A, 228, 519–538, 1955.

Gogineni, P.: CReSIS Radar Depth Sounder Data, http://data.cresis.ku.edu/, 2012.

Holland, P. R., Jenkins, A., and Holland, D. M.: The response of ice shelf basal melting to variations in ocean temperature, J. CLim, 21, 2558–2572, doi:10.1175/2007JCLI1909.1, 2008.

Hughes, T.: The weak underbelly of the West Antarctic ice-Sheet, Journal of Glaciology, 27, 518–525, 1981.

Humbert, A. and Steinhage, D.: The evolution of the western rift area of the Fimbul Ice Shelf, Antarctica, The Cryosphere, 5, 931–944, doi:10.5194/tc-5-931-2011, http://www.the-cryosphere.net/5/931/2011/, 2011.

Jacobs, S. S., Jenkins, A., Giulivi, C. F., and Dutrieux, P.: Stronger ocean circulation and increased melting under Pine Island Glacier ice shelf, Nature Geosci., 4, 519–523, doi:10.1038/NGEO1188, 2011.

Jenkins, A., Dutrieux, P., Jacobs, S., McPhail, S., Perrett, J., Webb, A., and White, D.: Observations beneath Pine Island Glacier in West Antarctica and implications for its retreat, Nature Geosci., 3, 468–472, 2010.

Joughin, I., Smith, B. E., Howat, I. M., Floricioiu, D., Alley, R. B., Truffer, M., and Fahnestock, M.: Seasonal to decadal scale variations in the surface velocity of Jakobshavn Isbrae, Greenland: Observation and model-based analysis, J. Geophys. Res., 117, 1–20, doi:10.1029/2011JF002110, 2012.

Joughin, I., Smith, B. E., and Medley, B.: Marine ice sheet collapse potentially under way for the Thwaites Glacier Basin, West Antarctica., Science (New York, N.Y.), 344, 735–8, doi:10.1126/science.1249055, 2014.

Krabill, W.: IceBridge ATM L2 Icessn Elevation, Slope, and Roughness, Version 2, 2014.

Krug, J., Weiss, J., Gagliardini, O., and Durand, G.: Combining damage and fracture mechanics to model calving, The Cryosphere, 8, 2101–2117, doi:10.5194/tc-8-2101-2014, 2014.

Krug, J., Durand, G., Gagliardini, O., and Weiss, J.: Modelling the impact of submarine frontal melting and ice mélange on glacier dynamics, The Cryosphere Discussions, 9, 183–221, doi:10.5194/tcd-9-183-2015, 2015.

Larour, E., Rignot, E., and Aubry, D.: Processes involved in the propagation of rifts near Hemmen Ice Rise, Ronne Ice Shelf, Antarctica, J. Glaciol., 50, 329–341, 2004a.

Larour, E., Rignot, E., and Aubry, D.: Modelling of rift propagation on Ronne Ice Shelf, Antarctica, and sensitivity to climate change, Geophys. Res. Lett., 31, 1–4, doi:10.1029/2004GL020077, 2004b.

Larour, E., Seroussi, H., Morlighem, M., and Rignot, E.: Continental scale, high order, high spatial resolution, ice sheet modeling using the Ice Sheet System Model (ISSM), J. Geophys. Res., 117, 1–20, doi:10.1029/2011JF002140, 2012.

Lenaerts, J. T. M., van den Broeke, M. R., van de Berg, W. J., van Meijgaard, E., Kuipers Munneke, P., and Munneke, P. K.: A new, high-resolution surface mass balance map of Antarctica (1979-2010) based on regional atmospheric climate modeling, Geophys. Res. Lett., 39, 1–5, doi:10.1029/2011GL050713, 2012.

MacAyeal, D. R.: Large-scale ice flow over a viscous basal sediment: Theory and application to Ice Stream B, Antarctica, J. Geophys. Res., 94, 4071–4087, 1989.

MacGregor, J. A., Catania, G. A., Markowski, M. S., and Andrews, A. G.: Widespread rifting and retreat of ice-shelf margins in the eastern Amundsen Sea Embayment between 1972 and 2011, J. Glaciol., 58, 458–466, 2012.

MacGregor, J. A., Catania, G. A., Conway, H., Schroeder, D. M., Joughin, I., Young, D. A., Kempf, S. D., and Blankenship, D. D.: Weak bed control of the eastern shear margin of Thwaites Glacier, West Antarctica, Journal of Glaciology, 59, 900–912, doi:10.3189/2013JoG13J050, 2013.

Maule, C. F., Purucker, M. E., Olsen, N., and Mosegaard, K.: Heat Flux Anomalies in Antarctica Revealed by Satellite Magnetic Data, Science, 309, 464–467, 2005.

Morlighem, M., Rignot, E., Seroussi, H., Larour, E., Ben Dhia, H., and Aubry, D.: Spatial patterns of basal drag inferred using control methods from a full-Stokes and simpler models for Pine Island Glacier, West Antarctica, Geophysical Research Letters, 37, L14 502, 2010.

Morlighem, M., Rignot, E., Seroussi, H., Larour, E., Ben Dhia, H., and Aubry, D.: A mass conservation approach for mapping glacier ice thickness, Geophys. Res. Lett., 38, 1–6, doi:10.1029/2011GL048659, 2011.

Morlighem, M., Seroussi, H., Larour, E., and Rignot, E.: Inversion of basal friction in Antarctica using exact and incomplete adjoints of a higher-order model, J. Geophys. Res., 118, 1746–1753, doi:10.1002/jgrf.20125, 2013.

Mouginot, J., Rignot, E., and Scheuchl, B.: Sustained increase in ice discharge from the Amundsen Sea Embayment, West Antarctica, from 1973 to 2013, Geophys. Res. Lett., 41, 1–9, doi:10.1002/2013GL059069, 2014.

Nick, F. M., Vieli, A., Andersen, M. L., Joughin, I., Payne, A., Edwards, T. L., Pattyn, F., and van de Wal, R. S. W.: Future sea-level rise from Greenland's main outlet glaciers in a warming climate, Nature, 497, 235–238, 2013.

Nowicki, S. M. J. and Wingham, D. J.: Conditions for a steady ice sheet–ice shelf junction, Earth Planet. Sci. Lett., 265, 246–255, doi:10.1016/j.epsl.2007.10.018, 2008.

Nye, J. F.: The distribution of stress and velocity in glaciers and ice-sheets, Proc. R. Soc. A, 239, 113–133, 1957.

O'Leary, M. and Christoffersen, P.: Calving on tidewater glaciers amplified by submarine frontal melting, Cryosphere, 7, 119–128, doi:10.5194/tc-7-119-2013, 2013.

Parizek, B. R., Christianson, K., Anandakrishnan, S., Alley, R. B., Walker, R. T., Edwards, R. a., Wolfe, D. S., Bertini, G. T., Rinehart, S. K., Bindschadler, R. a., and Nowicki, S. M. J.: Dynamic (in)stability of Thwaites Glacier, West Antarctica, J. Geophys. Res., 118, 1–18, doi:10.1002/jgrf.20044, 2013.

Pattyn, F.: A new three-dimensional higher-order thermomechanical ice sheet model: Basic sensitivity, ice stream development, and ice flow across subglacial lakes, J. Geophys. Res., 108, 1–15, doi:10.1029/2002JB002329, 2003.

Pattyn, F., Schoof, C., Perichon, L., Hindmarsh, R. C. a., Bueler, E., de Fleurian, B., Durand, G., Gagliardini, O., Gladstone, R., Goldberg, D., Gudmundsson, G. H., Huybrechts, P., Lee, V., Nick, F. M., Payne, a. J., Pollard, D., Rybak, O., Saito, F., and Vieli, A.: Results of the Marine Ice Sheet Model Intercomparison Project, MISMIP, The Cryosphere, 6, 573–588, doi:10.5194/tc-6-573-2012, http://www.the-cryosphere.net/6/573/2012/, 2012.

Plate, C., Müller, R., Humbert, A., and Gross, D.: Evaluation of the criticality of cracks in ice shelves using finite element simulations, The Cryosphere, 6, 973–984, doi:10.5194/tc-6-973-2012, http://www.the-cryosphere.net/6/973/2012/, 2012.

Pritchard, H. D., Arthern, R. J., Vaughan, D. G., and Edwards, L. A.: Extensive dynamic thinning on the margins of the Greenland and Antarctic ice sheets, Nature, 461, 971–975, doi:10.1038/nature08471, 2009.

Rignot, E.: Evidence for rapid retreat and mass loss of Thwaites Glacier, West Antarctica, J. Glaciol., 47, 213–222, doi:10.3189/172756501781832340, 2001.

Rignot, E.: Changes in West Antarctic ice stream dynamics observed with ALOS PALSAR data, Geophys. Res. Lett., 35, 1–5, doi:10.1029/2008GL033365, 2008.

Rignot, E. and Jacobs, S. S.: Rapid bottom melting widespread near Antarctic ice sheet grounding lines, Science, 296, 2020–2023, doi:10.1126/science.1070942, 2002.

Rignot, E., Koppes, M., and Velicogna, I.: Rapid submarine melting of the calving faces of West Greenland glaciers, Nat. Geosci., 3, 187–191, doi:10.1038/NGEO765, 2010.

Rignot, E., Mouginot, J., and Scheuchl, B.: Antarctic grounding line mapping from differential satellite radar interferometry, Geophysical Research Letters, 38, n/a–n/a, doi:10.1029/2011GL047109, 2011a.

Rignot, E., Mouginot, J., and Scheuchl, B.: Ice Flow of the Antarctic Ice Sheet, Science, 333, 1427–1430, doi:10.1126/science.1208336, 2011b.

Rignot, E., Jacobs, S., Mouginot, J., and Scheuchl, B.: Ice shelf melting around Antarctica, Science, 341, 266–270, doi:10.1126/science.1235798, 2013.

Rignot, E., Mouginot, J., Morlighem, M., Seroussi, H., and Scheuchl, B.: Widespread, rapid grounding line retreat of Pine Island, Thwaites, Smith and Kohler glaciers, West Antarctica from 1992 to 2011, Geophys. Res. Lett., in press, 2014.

Rist, M., Sammonds, P., Murrell, S., Meredith, P., Oerter, H., and Doake, C.: Experimental fracture and mechanical properties of Antarctic ice: preliminary results, Annals of Glaciology, 23, 284–292, 1996.

Rist, M. A., Sammonds, P. R., Oerter, H., and Doake, C. S. M.: Fracture of Antarctic shelf ice, J. Geophys. Res., 107, 1–13, doi:10.1029/2000JB000058, 2002.

Schoof, C.: Ice sheet grounding line dynamics: Steady states, stability, and hysteresis, J. Geophys. Res., 112, 1–19, doi:10.1029/2006JF000664, 2007.

Seroussi, H., Morlighem, M., Rignot, E., Larour, E., Aubry, D., Ben Dhia, H., and Kristensen, S. S.: Ice flux divergence anomalies on 79north Glacier, Greenland, Geophys. Res. Lett., 38, 1–5, 2011.

Seroussi, H., Ben Dhia, H., Morlighem, M., Rignot, E., Larour, E., and Aubry, D.: Coupling ice flow models of varying order of complexity with the Tiling Method, J. Glaciol., 58 (210), 776–786, doi:10.3189/2012JoG11J195, 2012.

Seroussi, H., Morlighem, M., Rignot, E., Khazendar, A., Larour, E., and Mouginot, J.: Dependence of century-scale projections of the Greenland ice sheet on its thermal regime, J. Glaciol., 59, 1024–1034, doi:10.3189/2013JoG13J054, 2013.

Seroussi, H., Morlighem, M., Larour, E., Rignot, E., and Khazendar, A.: Hydrostatic grounding line parameterization in ice sheet models, The Cryosphere, 8, 2075–2087, 2014.

Shepherd, A., Wingham, D., and Mansley, J.: Inland thinning of the Amundsen Sea sector, West Antarctica, Geophysical Research Letters, 29, 7–10, 2002.

Shepherd, A., Ivins, E. R., A, G., Barletta, V. R., Bentley, M. J., Bettadpur, S., Briggs, K. H., Bromwich, D. H., Forsberg, R., Galin, N., Horwath, M., Jacobs, S., Joughin, I., King, M. a., Lenaerts, J. T. M., Li, J., Ligtenberg, S. R. M., Luckman, A., Luthcke, S. B., McMillan, M., Meister, R., Milne, G., Mouginot, J., Muir, A., Nicolas, J. P., Paden, J., Payne, A. J., Pritchard, H., Rignot, E., Rott, H., Sø rensen, L. S., Scambos, T. a., Scheuchl, B., Schrama, E. J. O., Smith, B., Sundal, A. V., van Angelen, J. H., van de Berg, W. J., van den Broeke, M. R., Vaughan, D. G., Velicogna, I., Wahr, J., Whitehouse, P. L., Wingham, D. J., Yi, D., Young, D., and Zwally, H. J.: A reconciled estimate of ice-sheet mass balance., Science (New York, N.Y.), 338, 1183–9, 2012.

Spence, P., Griffie, S. M., England, M. H., Hogg, A. M., Saenko, O. A., and Jourdain, N. C.: Rapid subsurface warming and circulation changes of Antarctic coastal waters by poleward shifting winds, Geophys. Res. Lett., 41, 4601–4610, doi:10.1002/2014GL060613.Received, 2014.

Tinto, K. J. and Bell, R. E.: Progressive unpinning of Thwaites Glacier from newly identified offshore ridge: Constraints from aerogravity, Geophys. Res. Lett., 38, 1–5, doi:10.1029/2011GL049026, 2011.

van der Veen, C. J.: Fracture mechanics approach to penetration of bottom crevasses on glaciers, Cold Reg. Sci. Technol., 27, 213–223, 1998a.

van der Veen, C. J.: Fracture mechanics approach to penetration of surface crevasses on glaciers, Cold Reg. Sci. Technol., 27, 31–47, 1998b.

van der Veen, C. J. and Whillans, I. M.: Force budget: I. Theory and numerical methods, J. Glaciol., 35, 53–60, 1989.

Van der Veen, C. J. and Whillans, I. M.: Model experiments on the evolution and stability of ice streams, Annals of Glaciology, 23, 129–137, 1996.

Vaughan, D. G., Corr, H. F. J., Bindschadler, R. A., Dutrieux, P., Gudmundsson, G. H., Jenkins, A., Newman, T., Vornberger, P., and Wingham, D. J.: Subglacial melt channels and fracture in the floating part of Pine Island Glacier, Antarctica, J. Geophys. Res. - Earth Surface, 117, doi:10.1029/2012JF002360, 2012.

Vieli, A. and Payne, A. J.: Assessing the ability of numerical ice sheet models to simulate grounding line migration, Journal of Geophysical Research, 110, F01 003, doi:10.1029/2004JF000202, 2005.

Vogel, C. R.: Computational Methods for Inverse Problems, Society for Industrial and Applied Mathematics, Philadelphia, PA, USA, 2002.

Weertman, J.: Stability of the junction of an ice sheet and an ice shelf, J. Glaciol., 13(67), 3–11, 1974.

Table 1. ~~Experiments~~ Experiment characteristics

Experiment Set	Number of Experiments	Experiment
~~Ma~~ A	~~4 Control melt rate plus additional melt rateMb 4 Steady state melt rate plus additional melt rateCa~~ 11	Current geometry wit
~~Cb~~ B	7	~~3 m initial surface cre~~
~~Cd~~ C	4	2 km
~~Ce~~ D	7	3 m initial s
E	7	4 km ice shelf with 400 m l

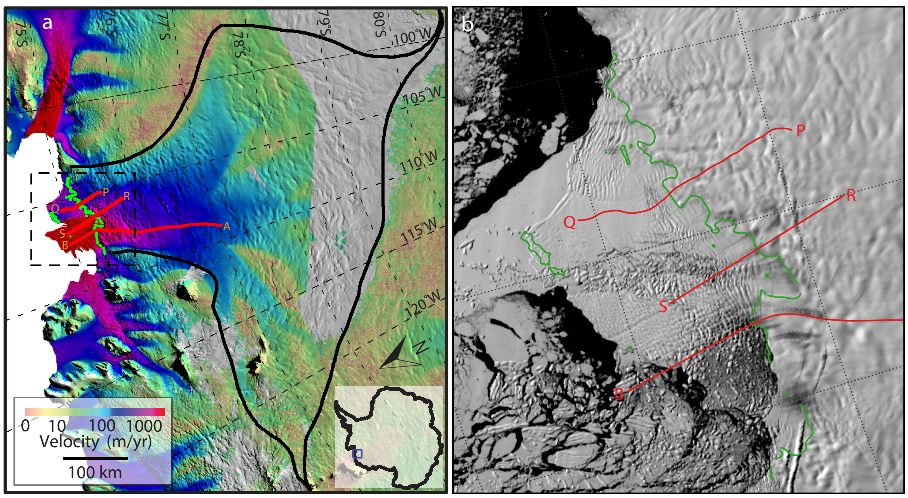

Figure 1. Velocity map and MODIS image of Thwaites Glacier (TG), West Antarctica. a) Velocity field of TG derived from InSAR with data collected in 2008 (Rignot et al., 2011b). The black contour is the drainage basin of TG. ~~Dashed box is the region of the~~ b) MODIS image of the dashed box region in ~~Fig~~a) on Nov. ~~2a~~01, 2012. PQ and RS are the flight tracks of ~~echogram~~ the echograms shown in Fig. ~~2b and 2c.~~ 2. AB is the selected flowline of this study. The green line is the grounding line of TG in 2011 (Rignot et al., 2011a).

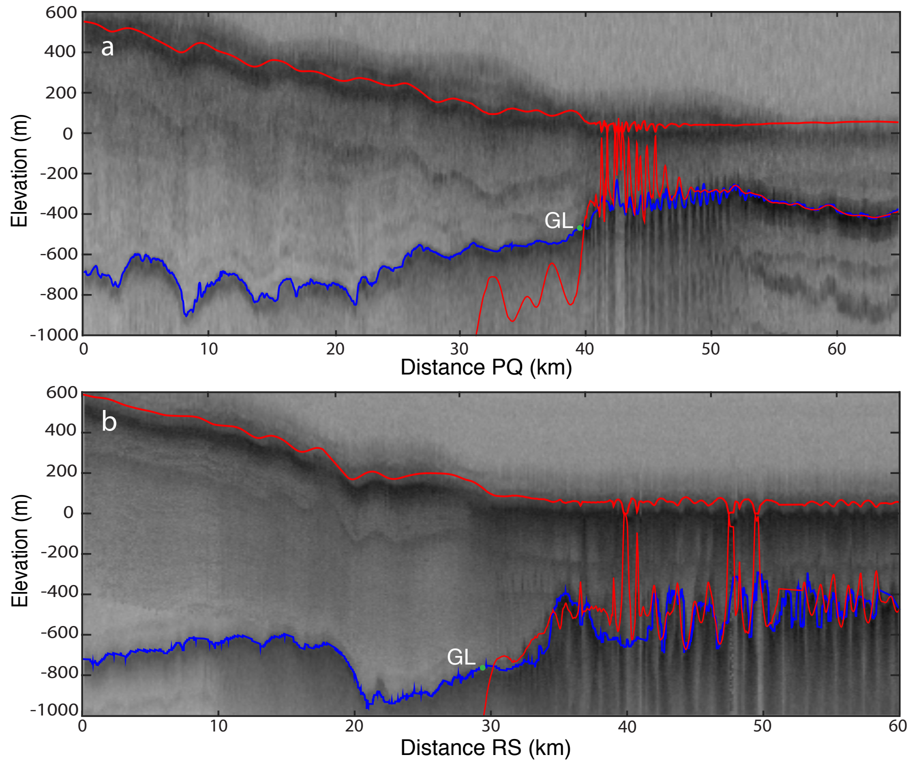

Figure 2. ~~a) MODIS image~~ Two echograms of ~~TG on Jan.15, 2013. The green line~~ Thwaites Glacier (~~a~~TG)~~and dots (b and c) are the grounding line positions~~. ~~b~~a) Echogram of flight track PQ on Nov.02, 2009. ~~c~~b) Echogram of flight track RS on Nov.19, ~~2011.~~ 2010. The red ~~solid~~ lines are ice surface elevation measured ~~from~~ by Airborne Topographic Mapper (ATM) (Krabill, 2014) and ~~the red dashed lines are~~ bed elevation calculated from hydrostatic equilibrium. The blue ~~line is~~ lines are the elevation of ice bottom measured ~~from~~ by ice radar depth sounder (Gogineni, 2012). The green dots are the grounding line positions in 2011 (Rignot et al., 2011a).

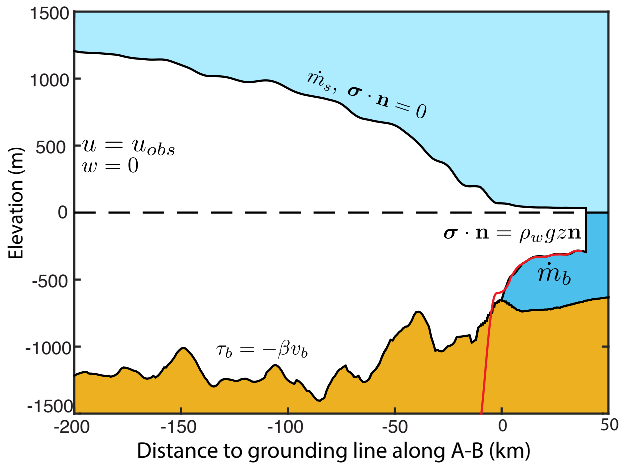

Figure 3. Geometry of the selected flowline ~~A-B in Fig. 1~~ AB and boundary conditions of the model. The black lines are ice surface elevation, ice bottom elevation and bed elevation. The red line is the hydrostatic bed calculated from surface elevation

~~Comparison of lateral drag, longitudinal drag, basal drag and driving stress along flowline A-B over a length scale of 5 km.~~

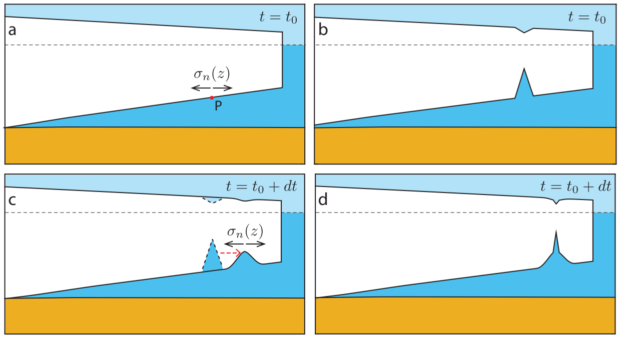

Figure 4. ~~Algorithm for~~ Schematic of the combination of ISSM and ~~the~~ LEFM~~model~~. a) Initial condition, b) Crevasses propagate, c) Crevasses advect downstream, d) Crevasses grow.

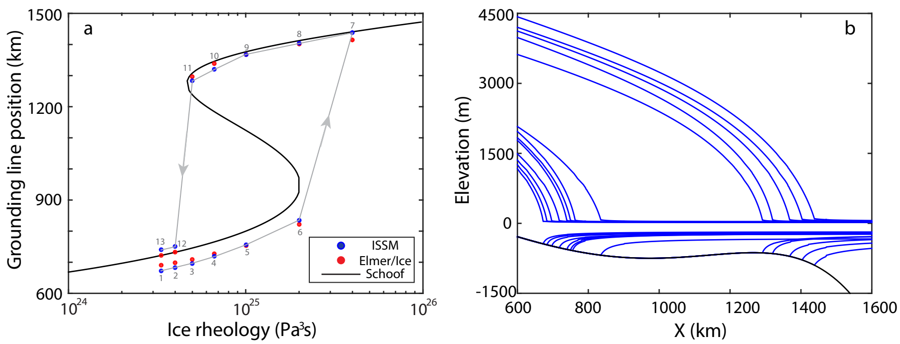

Figure 5. Results of MISMIP Exp 3. a) Steady state grounding line positions of MISMIP Exp 3 obtained by ISSM (blue dots) compared with the FS solution of Elmer/Ice Durand et al. (2009a) (red dots) and Schoof (2007) solution (black curve) (Pattyn et al., 2012). The gray arrow shows the sequence of ice rheology perturbation at each step. b) Steady state profile at each step obtained by ISSM

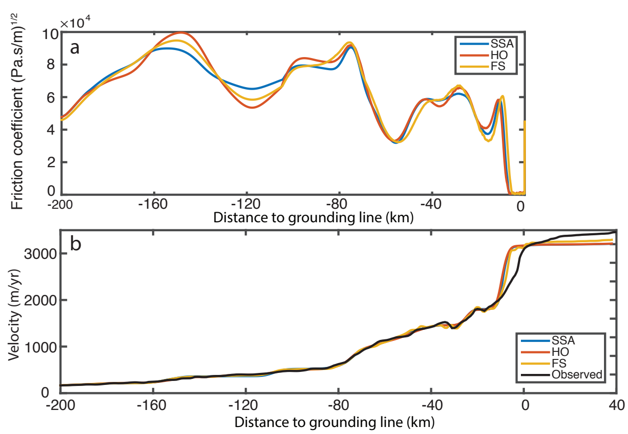

Figure 6. Inversion results of basal friction on flowline AB. a) Friction coefficient inferred with all three models (FS, HO and SSA). b) Comparison of modeled surface velocity and observed surface velocity for all three models.

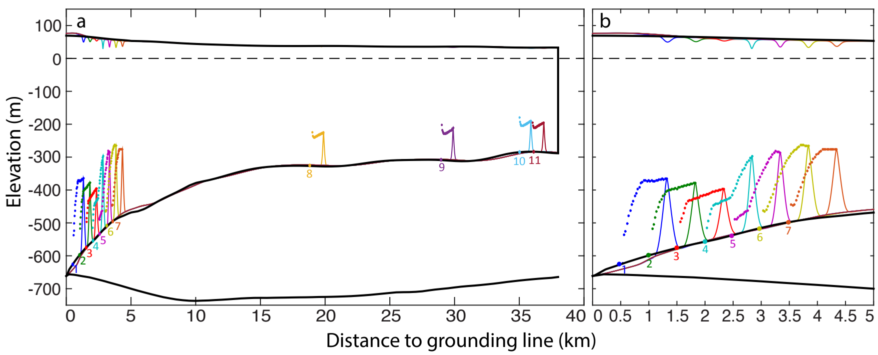

Figure 7. ~~a) Basal melt rate required to achieve steady state solution at current~~ Crevasse propagation with the initial geometry ~~for all three models~~of flowline AB. ~~b~~a) ~~Flowline geometry~~ Crevasse propagation of ~~all three models at~~ Exp. A1–A11 with FS. Each color corresponds to one initial crevasse position, indicated by the ~~end of the simulations~~number. ~~Black~~ The solid lines are the ~~current observed geometry~~shape of final crevasses. ~~Evolution~~ The dotted lines are the evolution of ~~flowline geometry~~ the tips of ~~Exp~~bottom crevasses. ~~Ma1–Ma4. a) Basal melt rate for each experiment.~~ b) ~~Final geometry~~ Details of ~~FS experiments~~the grounding line region for Exp. ~~c) Final geometry of HO experiments~~A1-A7. ~~d) Final~~ The black lines are the initial geometry ~~of SSA experiments~~for ice surface, ice bottom and seafloor.

~~Evolution of flowline geometry for Exp. Mb1–Mb4. Upper panels are the basal melt rate for each experiment and lower panels are the final geometry profiles for FS, HO and SSA, respectively. Crevasse propagation of Exp. Ca1–Ca11 with FS. Each color corresponds to one initial crevasse position, indicated by the number. The solid lines are final crevasse shape and the dotted lines are the evolution of the tip of bottom crevasses.~~

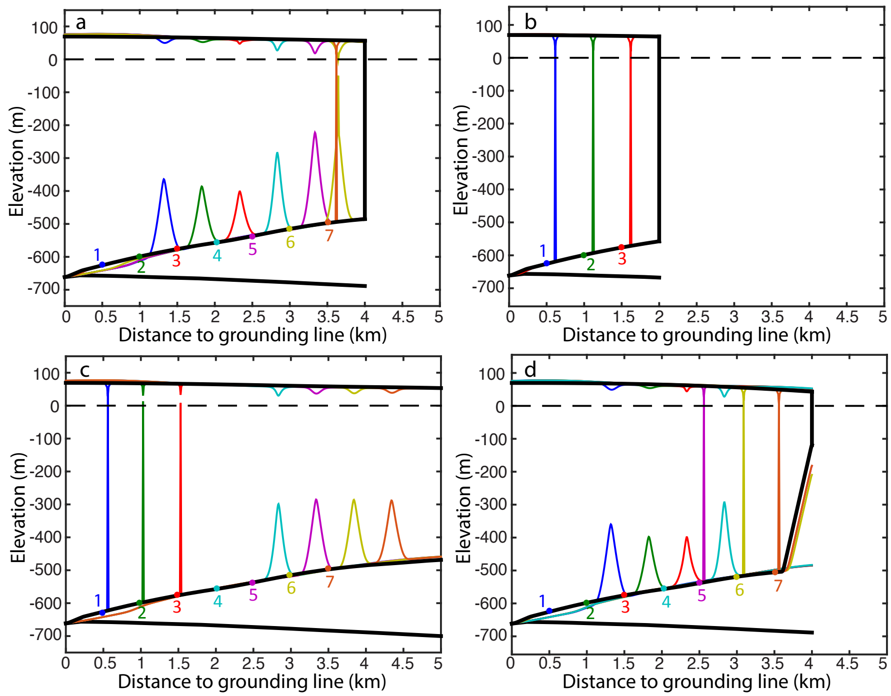

Figure 8. Crevasse propagation in the grounding line region with varying initial geometry. In each panel, ~~dashed~~ solid lines are the ~~final crevasses~~ shape ~~from the initial geometry (Exp. Ca1–Ca11). Solid lines are~~ of final crevasses ~~shape~~ with a) ~~3 m initial surface crevasse~~ 4 km long ice shelf (Exp. ~~Cb1–Cb7~~B1–B7), b) ~~4~~ 2 km long ice shelf (Exp. ~~Cc1–Cc7~~C1–C3), c) ~~2 km ice shelf~~ 3 m deep, 100 m wide initial surface crevasse (Exp. ~~Cd1–Cd3~~D1–D7), and d) 4 km long ice shelf with a 400 m wide and 400 m high ~~undercutting~~ undercut ice front (Exp. ~~Ce1–Ce7~~E1–E7). The ~~grey~~ black lines ~~in b, c and d~~ are the initial geometry for ice ~~front positions~~surface, ice bottom and seafloor.